Materials Today Bio 30 (2025) 101406

Contents lists available at ScienceDirect

Materials Today Bio

journal homepage: www.journals.elsevier.com/materials-today-bio

Macrophage-mimicking nanotherapy for attenuation of acute pancreatitis

Fengyu Shi [a,b,c,d,1], Akmal Ergashev [b,c,d,1], Zhenyan Pan [b,c,d,1], Hongwei Sun [b,c,d,1], Lingming Kong [b,c,d], Yuepeng Jin [b,c,d], Tan Zhang [b,c,d], Zhu Liu [b,c,d], Haonan Xie [b,c,d], Jinhui Wang [b,c,d], Huiping Li [b,c,d], Yi Wang [e], Lifei Zheng [f], Jianliang Shen [g,h], Andreas Herrmann [d,i,j,***], Gang Chen [b,c,d,**], Hongru Kong [b,c,d,*]

[a] Department of Radiology, The First Affiliated Hospital of Wenzhou Medical University, Wenzhou, Zhejiang, 325035, China
[b] Department of Hepatobiliary Surgery, The First Affiliated Hospital of Wenzhou Medical University, Wenzhou, Zhejiang, 325035, China
[c] Zhejiang Key Laboratory of intelligent Cancer Biomarker Discovery & Translation, The First Affiliated Hospital of Wenzhou Medical University, Zhejiang, 325035, China
[d] Zhejiang-Germany Interdisciplinary Joint Laboratory of Hepatobiliary-Pancreatic Tumor and Bioengineering, Wenzhou, Zhejiang, 325035, China
[e] Department of Epidemiology and Biostatistics, School of Public Health and Management, Wenzhou Medical University, Wenzhou, 325000, China
[f] Wenzhou Institute, University of Chinese Academy of Sciences, Wenzhou, 325001, China
[g] National Engineering Research Center of Ophthalmology and Optometry, Eye Hospital, Wenzhou Medical University, Wenzhou, 325027, China
[h] Zhejiang Engineering Research Center for Tissue Repair Materials, Wenzhou Institute, University of Chinese Academy of Sciences, Wenzhou, 325001, China
[i] DWI – Leibniz-Institute for Interactive Materials, Aachen, 52056, Germany
[j] Institute for Technical and Macromolecular Chemistry, Rheinisch-Westfälische Technische Hochschule (RWTH) Aachen University, Aachen, 52074, Germany

ARTICLE INFO

Keywords:
Acute pancreatitis
Macrophage-mimicking nanotherapy
Selenylated Poria cocos polysaccharide nanoparticles
AKT/mTOR pathway
Autophagy

ABSTRACT

Acute pancreatitis (AP) is a highly fatal pancreatic inflammation. In recent years, synthetic nanoparticles have been extensively developed as drug carriers to address the challenges of systemic adverse reactions and lack of specificity in drug delivery. However, systemically administered nanoparticle therapy is rapidly cleared from circulation by the mononuclear phagocyte system (MPS), leading to suboptimal drug concentrations in inflamed tissues and suboptimal pharmacokinetics. To address this challenge, we herein demonstrate a surface masking strategy that involves coating the surface of selenylated Poria cocos polysaccharide nanoparticles with a layer of macrophage plasma membrane to circumvent MPS sequestration, thereby enhancing the therapeutic efficacy of selenylated Poria cocos polysaccharide nanoparticles. Nanoparticles encapsulated with macrophage membranes can simulate the active homing efficacy of macrophages to inflamed lesions during AP, resulting in excessive infiltration of macrophages in pancreatic inflammation sites and prolonged tissue retention time. This technique converts non-adhesive lipid nanoparticles into bioadhesive nanoparticles, increasing local tissue accumulation under inflammatory conditions, including the pancreas and vulnerable lungs. The mechanism is related to targeting pro-inflammatory macrophages. In murine models of mild and severe AP, intravenous treatment with macrophage-mimicking nanoparticles effectively reduces systemic inflammation level and diminishes the recruitment of macrophages and neutrophils. Mechanistic studies elucidate that macrophage membrane-biomimetic selenylated Poria cocos polysaccharide nanoparticles primarily mitigate pancreatic inflammation by inhibiting the AKT/mTOR pathway to reverse autophagic flux impairment. This allows us to envision that the developed biomimetic nanotherapy approach could potentially serve as a novel strategy for pancreatic drug therapy.

* Corresponding author. Department of Hepatobiliary Surgery, The First Affiliated Hospital of Wenzhou Medical University, Wenzhou, Zhejiang, 325035, China.
** Corresponding author. Department of Hepatobiliary Surgery, The First Affiliated Hospital of Wenzhou Medical University, Wenzhou, Zhejiang, 325035, China.
*** Corresponding author. Zhejiang-Germany Interdisciplinary Joint Laboratory of Hepatobiliary-Pancreatic Tumor and Bioengineering, Wenzhou, Zhejiang, 325035, China.
E-mail addresses: herrmann@dwi.rwth-aachen.de (A. Herrmann), chen.gang@wmu.edu.cn (G. Chen), konghongru@wmu.edu.cn (H. Kong).
[1] These authors contributed equally.

https://doi.org/10.1016/j.mtbio.2024.101406
Received 18 July 2024; Received in revised form 29 November 2024; Accepted 14 December 2024
Available online 15 December 2024

1. Introduction

Acute pancreatitis (AP) is an inflammatory disease caused by the premature activation of digestive enzymes in pancreatic acinar cells (PACs), with a potential risk of fatality [1–3]. The severity of AP spans a spectrum, roughly 20% of patients experience moderate or severe acute pancreatitis (SAP), with a significant mortality rate ranging from 20% to 40% [4–6]. Despite advancing comprehension of the underlying mechanisms of AP, effective pharmacological treatment remains elusive, with therapeutic strategies still predominantly relying on general anti-inflammatory approaches [7,8]. In recent years, there is growing evidence supporting the involvement of impaired autophagy and activation of inflammation in the pathogenesis of AP [9,10]. During the course of AP, intracellular autophagosomes accumulate and damaged mitochondria build up, leading to increased reactive oxygen species (ROS) production and accumulation of autophagy-related proteins (LC3

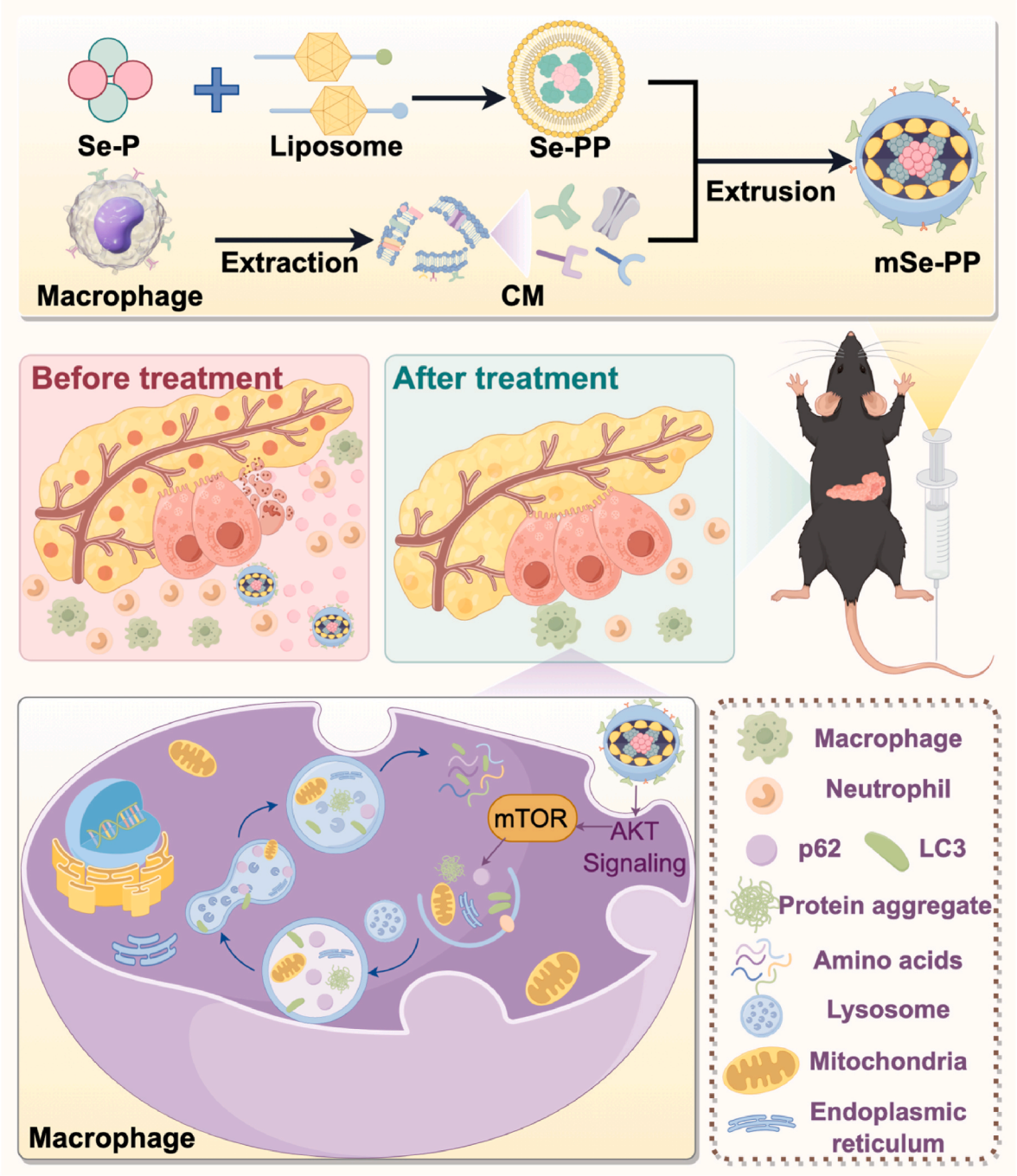

Scheme 1. Macrophage membrane-biomimetic selenylated Poria cocos polysaccharide nanoparticles attenuate acute pancreatitis injury. Firstly, selenylated Poria cocos polysaccharide nanoparticles (Se-P) formed uncoated selenylated Poria cocos polysaccharide lipid nanoparticles (Se-PP) by thin-film hydration method with liposomes, then further combined with extracted macrophage membrane (CM) proteins to form macrophage membrane-biomimetic selenylated Poria cocos polysaccharide nanoparticles (mSe-PP). Subsequently, different formulations were intravenously injected to treat acute pancreatitis in mice. mSe-PP accumulated in the pancreatic microenvironment of inflammation, interfering with the recruitment of macrophages and neutrophils. It alleviated the severity of inflammation by inhibiting the expression and secretion of pro-inflammatory factors in macrophages. Simultaneously, it reversed autophagy pathway damage by inhibiting the AKT/mTOR pathway in macrophages, thereby reducing the production of ROS and cell apoptosis.

and SQSTM1/p62), further damaging cells and disrupting cellular function [11]. Furthermore, evidence suggests that cellular autophagy is regulated by the AKT/mTOR pathway [12–15]. Therefore, modulating the AKT/mTOR-autophagy processes in drug development presents a potential strategy and perspective for treating AP.

Poria cocos polysaccharides (PCP) are considered as a vital component of Poria cocos (Schw.) Wolf [16]; however, in which, around 90% of polysaccharides are insoluble in water, exhibiting relatively weak biological activity [17]. Research indicates that the water solubility and bioavailability of polysaccharides could be further enhanced by appropriate chemical modifications [18]. Natural or synthetic selenium (Se)-enriched polysaccharides known for their heightened and unique biological activities, for example, have emerged in the treatment of acute liver injury, renal damage, and ulcerative colitis [19–21], such as anti-tumor effects, antioxidant properties, and immunomodulation [22–25]. Despite numerous studies suggesting the therapeutic potential between selenium-modified polysaccharides and inflammation [26,27], limited research has been conducted on the selenylation of PCP and the anti-inflammatory properties of selenylated Poria cocos polysaccharide nanoparticles (Se-P) in the context of pancreatitis [28].

The traditional free drug therapy is constrained by various drug performance parameters [29], whereas targeted drug delivery nanotherapies achieve efficient drug delivery through approaches such as internal biological stimuli (e.g., pH, enzyme expression and redox potential) [30,31], external stimuli (e.g., temperature, ultrasound, magnetic field and light) [32], immune cell targeting [33], and other innovative strategies. The integration of biomimetic nanomaterials into inflammatory disease research has seen rapid progress recently [34–36]. Based on the infiltration of innate immune cells, particularly macrophages, during the progression of AP leading to a high inflammatory state, macrophage-associated inflammatory responses may result in the progression of inflammation from local to systemic, and in severe cases, may lead to multi-organ dysfunction [37]. To address this, we developed nanoparticles that feature macrophage plasma membrane coating, effectively camouflaging selenylated polysaccharide nanoparticles. By preserving membrane components and antigens, these microparticles demonstrate specific neutralization of pathological molecules, prolonged circulation through immune evasion, and targeted accumulation at lesion sites [38], demonstrating their unique advantages as biomimetic carriers for drug delivery.

This study presents a targeted approach to enhance pancreatitis treatment by leveraging the selenylation modification of polysaccharides and biomimetic macrophage membrane cloaking strategies (Scheme 1). In both mild and severe AP mouse models, macrophage membrane-biomimetic anti-inflammatory nanoparticle (referred to as mSe-PP) is more effective in protecting the pancreas and reducing the severity of the disease compared to the uncoated lipid nanoparticles (referred to as Se-PP). Overall, mSe-PP serves as a distinctive biomimetic nanoparticle platform capable of delivering Se-P efficiently and has potential for the treatment of AP.

2. Materials and methods

2.1. Materials

1,2-dioleoyl-sn-glycero-3-phosphocholine (DOPC), 1,2-distearoyl-sn-glycero-3-phosphocholine (DSPC), 1,2-dipalmitoyl-sn-glycero-3-phosphocholine (DPPC) and cholesterol (CHOL) were obtained from CORDEN (Switzerland). Poria cocos polysaccharide was bought from Yuanye Biotechnology Co. Ltd. (Shanghai, China). Sodium selenite, ascorbic acid and lipopolysaccharide (Escherichia coli O127: B8) were purchased from Sigma-Aldrich (St. Louis, USA). Type IV collagenase and fetal bovine serum (FBS) were purchased from Gibco (USA). Antibodies against LC3B (ab192890), SQSTM1/p62 (ab109012), CD45 (ab40763), F4/80 (ab16911), MPO (ab9535), p-mTOR (ab109268) and lamin B1 (ab16048) were purchased from Abcam Inc. (Cambridge, MA, USA); p-AKT (4060) and AKT (4685) were purchased from Cell Signaling Technology Inc. (Beverly, MA, USA); GAPDH (60004-1-lg) and mTOR (66888-1-Ig) were purchased from Proteintech Inc. (Shanghai, China).

2.2. Preparation of selenylated Poria cocos polysaccharide nanoparticles

According to a previous report [39,40], Se-P was prepared using a chemical reduction method. After 12 h of reaction, the mixture was dialyzed (Mw cutoff: 14,000 Da) against ultrapure water for 24 h and then stored at 4°C.

2.3. Macrophage membrane (CM) isolation

A 2 mL volume of 3% thinoglycollate broth was intraperitoneally injected, recruiting circulating monocytes to the peritoneum, where they would transform into macrophages within 4 days. Peritoneal macrophages were cultured in DMEM medium supplemented with 10% fetal bovine serum and 1% penicillin/streptomycin. In vitro experiments used macrophage membranes from RAW264.7 cells, while others used peritoneal macrophage membranes from the mouse. The cell membrane was extracted by a reagent kit (Invent Biotechnologies, Inc., Plymouth, MN, USA).

2.4. Preparation of cell membrane-biomimetic nanoparticles

Liposomes were prepared by thin-film hydration accompanied by the extrusion method. The mixture of phospholipids with different head groups and cholesterol was dissolved in chloroform. The organic solvent was removed under reduced pressure at 60°C using a rotary evaporator. Then the lipid film was hydrated with 1 mL Se-P. The total lipid concentration of the liposomes was 20 mg/mL. 0.7 mg of extracted membrane proteins were mixed with 1 mL of Se-PP lipid nanoparticles. 0.1% (w/w) of coumarin 6 (Cou 6) or ICG was added for fluorescent labeling. The mixture was then extruded through polycarbonate membrane using an Avanti mini extruder (Avanti Polar Lipids Inc. Alabaster, AL, USA) with different pore sizes.

2.5. Characterization of nanoparticles

Mean particle diameter (z-average) and ζ-potential of liposomes were measured on a Malvern Zetasizer Nano-ZS (Malvern, UK) at 25°C. Liposomes were deposited on carbon-coated copper grids, negatively stained, and observed under a transmission electron microscope (JEM-2100Plus, Tokyo, Japan) at 80 kV. Fourier transformed infrared spectroscopy (FTIR) was measured by a fourier transformed infrared spectrometer (Nicolet iS10, Thermo Fisher Scientific, MA, USA).

2.6. Characterization of protein profile

RAW264.7 whole cell lysate, CM and Se-PP were loaded to 10% polyacrylamide gel for electrophoresis, and then stained with Coomassie blue before imaging with the BIO-RAD, Universal Hood II. For subsequent western blot analysis, the samples were processed according to the method described in the report [41].

2.7. Cumulative release

1 mL of liposome solutions were dialyzed (MWCO = 14 kDa) in 5 mL PBS (pH 7.4) with an oscillation rate of 120 rpm. 500 μL of release medium was collected at different time intervals and the released Se-P was determined by HPLC system (Shimadzu, Japan).

2.8. In vitro cellular uptake

HUVEC (Human Umbilical Vein Endothelial Cells) were activated with 10 ng/mL of tumor necrosis factor-alpha (TNF-α) for 6 h, and

RAW264.7 cells were activated with 1 μg/mL lipopolysaccharide (LPS) for 12 h. Subsequently, Cou 6-labeled nanoparticles were added and incubated for 30 min, followed by imaging under a fluorescence microscope and quantification by flow cytometry (FACS).

2.9. Animal experiments

This study utilized male specific pathogen-free (SPF) C57BL/6J mice (6–8 weeks of age) to establish AP models. All animal experiments were conducted in accordance with the guidelines outlined in the National Institute Guide for the Care and Use of Laboratory Animals. The experimental protocols received approval from the Ethics Committee of Wenzhou Medical University. Two distinct AP models were established in mice: FAEE-SAP (fatty acid ethyl ester-induced severe acute pancreatitis) and CAE-AP (caerulein-induced acute pancreatitis). For FAEE-SAP also known as alcohol-induced SAP: AP was induced by ethanol (1.3 g/kg) in combination with palmitoleic acid (POA) (150 mg/kg) twice intraperitoneally over 1 h. The mice had their serum, pancreatic, and lung samples collected at 12 h after the first injection. In the case of CAE-AP: AP was induced by 10 intraperitoneal injections of caerulein administered at a dose of 50 mg/kg at a 1 h interval, with samples collected from mice 24 h after the first injection.

2.10. Analysis of the organ distribution of nanoparticles in vivo using near-infrared (NIR) fluorescence imaging

ICG was employed as a NIR fluorescent probe. After the successful AP modeling, equal amounts of ICG-loaded Se-PP and mSe-PP were injected, respectively. Subsequently, the mice were anesthetized with isoflurane, and 0, 3, 12, 24 h after administration, whole-body fluorescent images were captured using the IVIS Spectrum (PerkinElmer, USA). After euthanasia, the major organs were isolated and imaged ex vivo.

2.11. Histopathology and immunofluorescence

Morphological changes were examined using hematoxylin and eosin (H&E) staining. Scoring was carried out independently by two researchers according to a standardised protocol and any discrepancies were resolved by a third researcher. For immunofluorescence staining, antigen repair was carried out in citric acid buffer. Endogenous peroxidase activity was blocked with 3% hydrogen peroxide, and then the sections were incubated with primary antibodies at 4°C overnight. The following antibodies were used: p-AKT (1:400), SQSTM1/p62 (1:100), LC3 (1:100), F4/80 (1:500), and CD45 (1:100). After washing, slides were incubated for 1 h with fluorescence-labeled secondary antibodies, followed by staining with 4,6-diamidino-2-phenylindole (DAPI).

2.12. Flow cytometry

Pancreatic tissues were digested in 1 ng/mL type IV collagenase solution (Gibco, USA) at 37°C. After 30 min, the digestion was terminated with DPBS containing 2% FBS and single cells were immediately filtered through a 75 μm filter. The cell suspension was stained with several monoclonal antibodies for 30 min at room temperature. The number of labeled cells was measured by flow cytometry (Beckman Coulter, Brea, CA, USA).

2.13. Statistical analysis

All data were presented as mean ± standard deviation (SD). ORIGIN software and GraphPad Prism 10 software platform were used for statistical analysis. A *t*-test was used for data with a normal distribution and comparisons between two groups. Single-factor analysis of variance (ANOVA) was used for comparison among the three groups. Semi-quantitative analysis of fluorescence images was carried out by Image J software. Scheme 1 was drawn using Figdraw. $P < 0.05$ indicates that the difference was statistically significant.

3. Results

3.1. Fabrication and characterization of membrane-biomimetic nanoparticles

Se-P lipid nanoparticles (Se-PP) and macrophage membrane-biomimetic Se-P lipid nanoparticles (mSe-PP) were included in the study. Under transmission electron microscopy (TEM), the dimensions of Se-PP and mSe-PP were about 100 nm and 110 nm, respectively (Fig. 1A and B). A monolayer cell membrane bilayer of about 10 nm was visible on the surface of mSe-PP compared with uncoated Se-PP, while dynamic light scattering (DLS) also showed that the average particle size of mSe-PP was about 20 nm larger than that of the bare Se-PP (Fig. 1C–E). CM was enriched with negatively charged membrane proteins and exhibited a negative ζ-potential, whereas Se-PP had a reduced ζ-potential due to cationic phospholipid modification. After CM modification, the negative charge of mSe-PP increased significantly, suggesting successful encapsulation of the membrane proteins in mSe-PP (Fig. 1F). The suitable size and negative potential of these nanoparticles prevent aggregation and promote their extended retention in tissue [42].

Proteins in the cytoplasmic membrane play a key role in the biocompatibility and targeting ability of nanoparticles. Therefore, we performed SDS-PAGE analysis to thoroughly verify whether the biomimetic nanomaterials inherited the biomarker profile of CM (Fig. 1G). Whole-cell lysates had a variety of protein components, after purification, the protein components of CM were reduced and mSe-PP displayed protein bands similar to CM. Obviously, mSe-PP inherited a very similar surface protein profile from macrophages, thus turning into bioadhesive biomimetic nanoparticles. Plasma membrane proteins, cytoplasmic proteins and nuclear membrane proteins were also assessed by western blot (Fig. 1H). The results showed that Na^+/K^+ ATPase and CD45, as representative membrane protein components, were abundant in both CM and mSe-PP, while IkBα, a representative cytoplasmic protein, was present in very low amounts in both CM and mSe-PP. Lamin B1 is a nuclear membrane protein marker, and no nuclear membrane protein was expressed in both CM and mSe-PP, indicating that CM were exclusively plasma membrane proteins.The Fourier transform infrared (FTIR) spectra of Se-P, Se-PP, and mSe-PP exhibited similar absorbance peaks, confirming the successful loading of Se-P (Fig. 1I). The encapsulation and loading efficiency of the Se-PP were 72.68 ± 2.53% and 1.45 ± 0.17%, in mSe-PP were 70.07 ± 3.06% and 1.27 ± 0.11%, respectively.

The stability of Se-PP and mSe-PP for storage in different media was assessed using DLS analysis. Both nanoparticles remained sufficiently stable in PBS or PBS containing FBS (10%, v/v) within one week (Figs. S1A and B). In vitro drug release was investigated in PBS buffer at pH 7.4, and both liposomes exhibited slow release characteristics (Fig. S1C). Further in vitro analysis of blood revealed that all nanoparticles induced hemolysis levels below 5% (Fig. 1J), indicating their biocompatibility within the bloodstream.

3.2. Cellular uptake of nanoparticles in vitro

The occurrence of AP involves various types of cells. Macrophages are among the immune cells that respond initially during AP phase [43], while endothelial cells contribute by producing and releasing inflammatory mediators, playing a key role in regulating the entire inflammatory response [44]. Next, we investigated the cellular uptake of Se-PP and mSe-PP separately in vitro using RAW264.7 cells (a macrophage cell line) and HUVEC (an endothelial cell line) as models, respectively. We assessed the uptake of Cou 6-labeled nanoparticles by non-stimulated and LPS-stimulated RAW264.7 cells. Compared to non-activated macrophages, activated macrophages exhibited significantly enhanced phagocytic activity toward Se-P and Se-PP (Fig. 2A-C). However, the

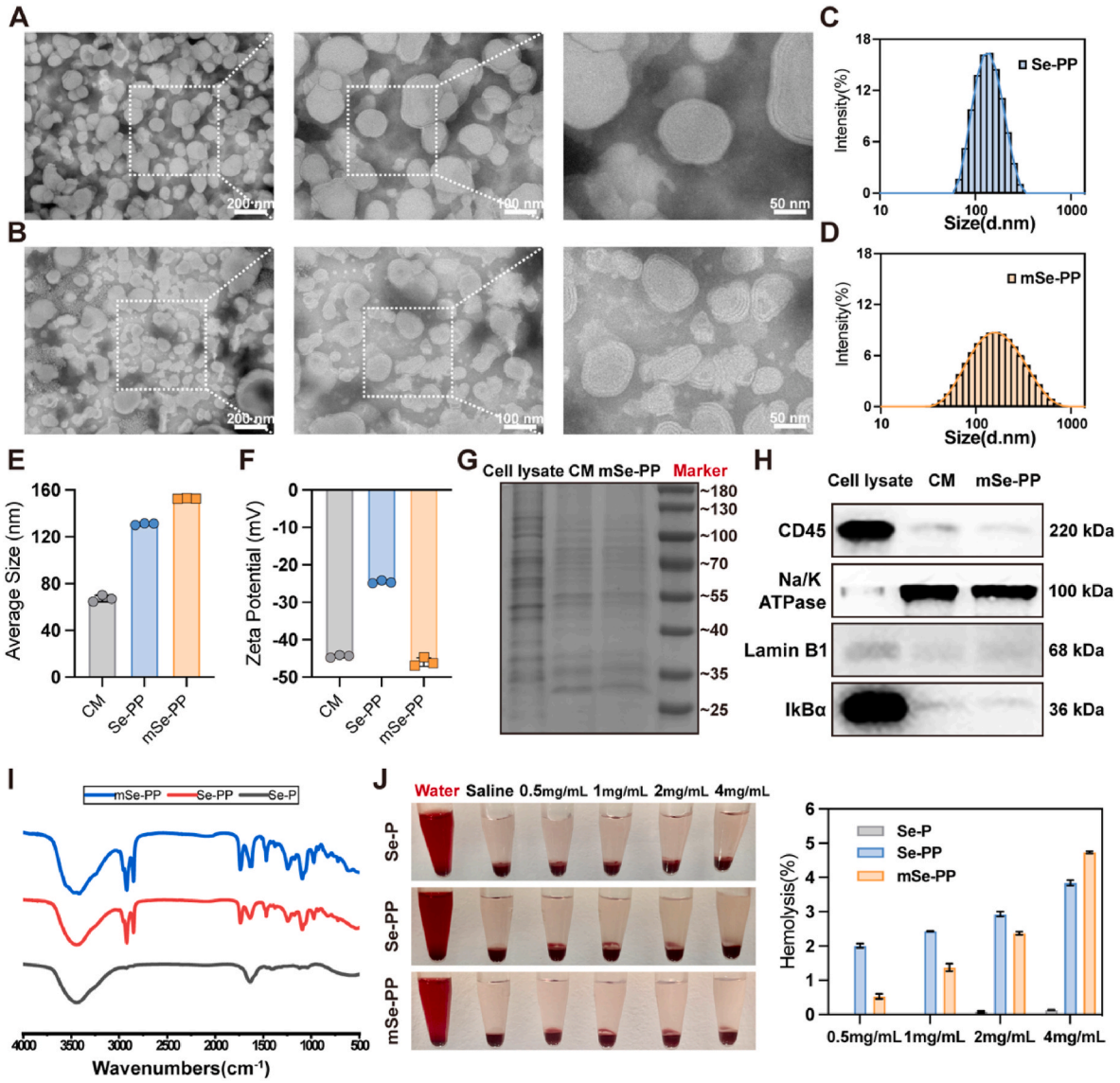

Fig. 1. Characterization of macrophage membrane-biomimetic selenylated Poria cocos polysaccharide nanoparticles. Transmission electron microscopy (TEM) images of (A) uncoated lipid nanoparticle (Se-PP) and (B) membrane-biomimetic nanoparticle (mSe-PP). Scale bars indicated 200 nm/100 nm/50 nm. (C, D) The size distribution, (E) hydrodynamic size (diameter, nm) and (F) zeta potential (ζ, mV) of nanoparticles measured using dynamic light scattering (DLS). (G) Protein profiles of RAW264.7 whole cell lysate, macrophage cell membrane (CM) and mSe-PP analyzed using SDS–PAGE. (H) Western blot assay of representative plasma membrane proteins, cytoplasmic protein and nuclear membrane proteins in whole cell lysate, CM, and mSe-PP. (I) The Fourier transform infrared (FTIR) spectra of Se-P, Se-PP, and mSe-PP dissolved in water. (J) The images of the centrifuged solutions containing erythrocytes after the incubation with Se-P, Se-PP, and mSe-PP, along with the quantification of the absorbance intensities of the supernatants. Erythrocytes treated with pure water were employed as the positive control. Each dot represents a sample (n = 3).

uptake of mSe-PP was significantly lower than that of Se-PP, regardless of whether the macrophages were activated or non-activated, possibly due to the reduction in positive charge to some extent caused by CM modification, resulting in repulsion with the negatively charged cell membrane, thereby reducing cellular uptake. The cellular uptake phenomenon observed in HUVEC was slightly different (Fig. 2D-F). Following stimulation with TNF-α, there was no difference in cellular uptake between normal HUVEC and activated HUVEC, suggesting that Se-PP and mSe-PP might have higher permeability to activated immune cells rather than activated endothelial cells. Similarly, consistent with the uptake observed in macrophage cell lines, the cellular uptake of mSe-PP in HUVEC was lower. In conclusion, Se-PP and mSe-PP were primarily absorbed by activated macrophages, thereby determining the targeting of subsequent anti-inflammatory therapy.

3.3. Macrophage-mimicking liposomes exhibited increased accumulation in the pancreas and lungs of SAP mice

Although cellular internalization experiments indicated that Se-PP and mSe-PP are predominantly taken up by pro-inflammatory macrophages, their in vivo targeting capability has not been validated. To address this, we labeled the nanoparticles with the NIR dye ICG to determine whether macrophage membrane-cloaked nanoparticles preferentially target inflammatory sites in vivo. We assessed the biodistribution of Se-PP and mSe-PP in the FAEE-SAP model.

Even within the 3 h observation period, the NIR fluorescence intensities gradually intensified over time in both nanotherapeutic-treated mice. Notably, mice in the mICG group showed more aggregated fluorescence signals in the pancreatic region, whereas the fluorescence signals of Se-PP were mainly concentrated in the liver (Fig. 2G). 3 h after

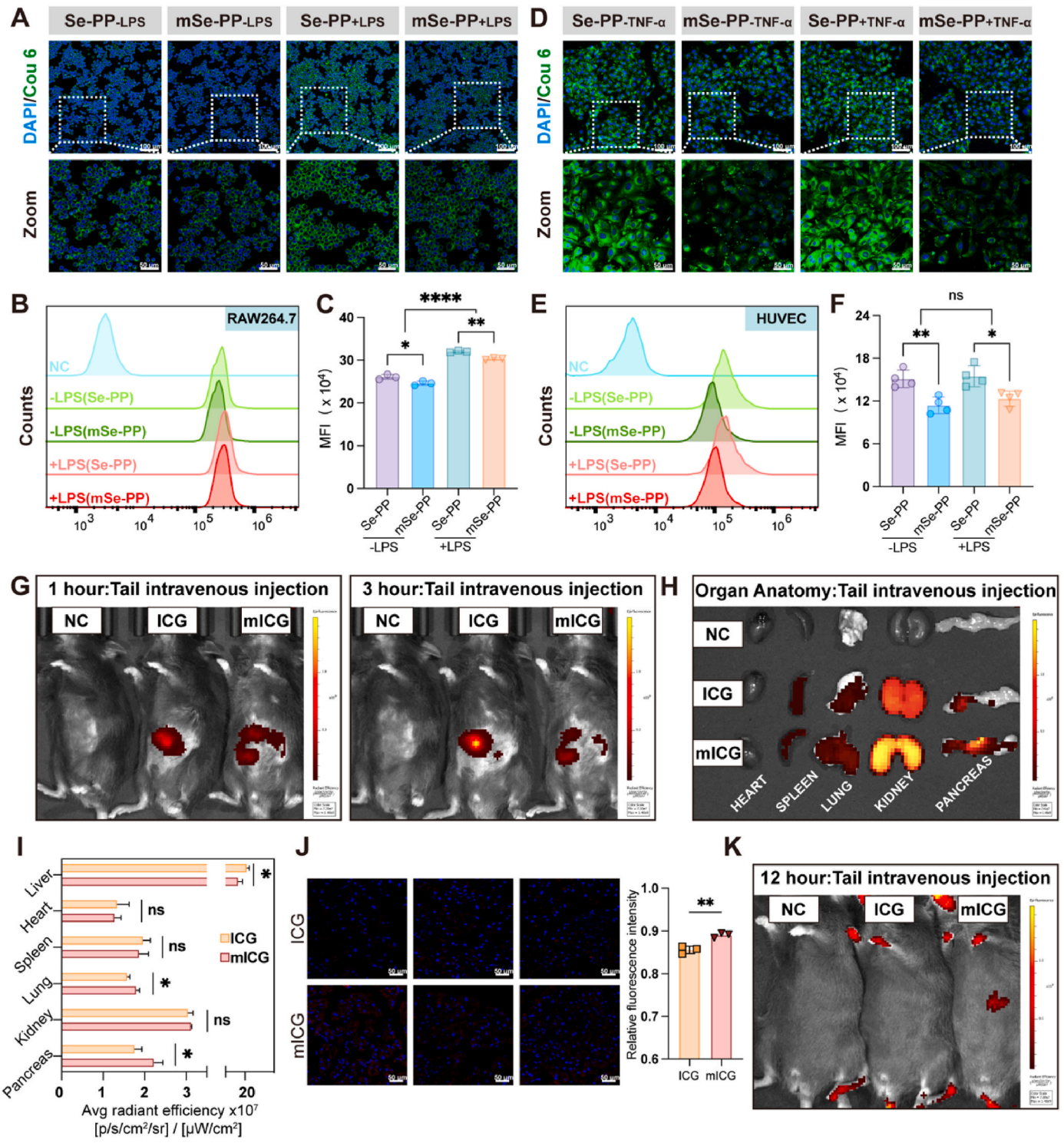

Fig. 2. Cellular uptake of nanoparticles in vitro and macrophage-mimicking liposomes exhibited increased accumulation in the pancreas and lungs of SAP mice. (A) Se-PP and mSe-PP uptake by RAW264.7 cells were examined using confocal laser microscopy. The nanoparticles were labeled with Cou 6 (green), and cell nuclei were stained with DAPI (blue). Scale bars indicated 100 μm/50 μm. (B–C) Uptake of the RAW264.7 cells after stimulation. Cells were stimulated with 1 μg/mL LPS prior to the incubation with Cou 6-labeled nanoparticles for 30 min at 37°C, and the fluorescence intensity was quantified by flow cytometry. (D) Se-PP and mSe-PP uptake by HUVEC were examined using confocal laser microscopy. (E–F) Uptake of the HUVEC after 10 ng/mL TNF-α stimulation. (G) Representative 1 h and 3 h in vivo NIR fluorescence images of SAP mice after intravenous injections of ICG-labeled nanoparticles. NC: negative control; ICG: ICG-labeled Se-PP; mICG: ICG-labeled mSe-PP. (H) Ex vivo fluorescence images of excised pancreas and other major organs (heart, spleen, lungs and kidneys) captured at 3 h post injection. (I) Quantitative analysis of the average radiant efficiency in major organs. (J) Fluorescence images and intensities of pancreatic sections visualized using confocal laser microscopy. The nanoparticles were labeled with ICG (red), and cell nuclei were stained with DAPI (blue). Scale bars, 50 μm. (K) Representative 12 h in vivo NIR fluorescence images of SAP mice after intravenous injections of ICG-labeled nanoparticles. Each dot represents a sample or mouse (n = 3–5). *p < 0.05, **p < 0.01, ***p < 0.001 and ****P < 0.0001.

injection, the major organs of the mice were imaged to evaluate the biodistribution of the nanoparticles. Quantitative data showed that the fluorescent drug in the mSe-PP group was primarily distributed in the liver, pancreas, lungs, and kidneys, while the signal for Se-PP was distributed in the liver, spleen, and kidneys (Fig. S2A and Figs. 2H, I). Additionally, we prepared frozen sections of pancreatic tissue from each group and conducted imaging using a confocal microscope. Our observations revealed that mSe-PP accumulated within the inflamed regions (Fig. 2J). This suggested that membrane cloaking by macrophage membranes enhances the inflammatory targeting capability of the nanotherapy.

Moreover, by extending the observation period, we observed that even 12 h post-administration, the fluorescence signal of mSe-PP in vivo attenuated more slowly compared to the Se-PP group (Fig. 2K), but the signal almost disappeared after 24 h of observation (Fig. S2B). This persistent fluorescence signal indicated that mSe-PP possesses superior tissue retention capability and a longer circulation time in the body. These properties were likely crucial for ensuring efficient delivery to the target inflammatory site and prolonging the nanoparticles' activity.

3.4. mSe-PP alleviated SAP and reduced inflammation in the pancreas and lungs

In the initial phase of our study, we determined that 16 mg/kg Se-P was the optimal concentration for animal experiments (Figs. S3A–D). Upon preparation, a uniform orange-red solution was observed (Figs. S3E and F); however, after 7 days, the uniformity of Se-P was disrupted, leading to the formation of aggregates (Fig. S3G). Additionally, Se-P showed suboptimal performance in both mild and severe models. These limitations restricted its potential applications (Fig. S4).

To evaluate the therapeutic effects and underlying mechanisms of Se-PP and mSe-PP in vivo, we performed a series of experiments utilizing the FAEE-SAP model, as shown in Fig. S5A. Gross morphology of the harvested pancreas revealed edema following the injection of fatty acid ethyl ester, which was alleviated after treatment, with mSe-PP showing more pronounced effects (Fig. S5C). Serum amylase and lipase levels were markedly elevated in FAEE-SAP mice, intravenous administration of mSe-PP resulted in a substantial reduction in these levels, whereas the efficacy of Se-PP was less pronounced (Fig. 3A and B). Consistent with the enzyme assays, both Se-PP and mSe-PP treatment groups exhibited decreased serum pro-inflammatory cytokines monocyte chemoattractant protein-1 (MCP-1), TNF-α, and interleukin-6 (IL-6) levels, with the mSe-PP-SAP group demonstrating a markedly higher reduction in comparison to the Se-PP-SAP group (Fig. 3C). These findings indicated that mSe-PP has a systemic inhibitory effect on the development of FAEE-SAP.

Subsequently, the therapeutic efficacy of mSe-PP at the tissue level was assessed by observing pathological changes in the pancreas [41,45]. In the SAP group, pancreatic tissue exhibited edema, inflammation, necrosis, and hemorrhage, with a higher pathological score. Following the administration of Se-PP and mSe-PP, the areas of inflammation, edema, necrosis, and hemorrhage were significantly reduced, resulting in lower pathological scores, particularly in the group receiving mSe-PP (Fig. 3D and G). Based on the aforementioned in vivo imaging, we found that the targeted accumulation of mSe-PP in the lungs is also noteworthy (Fig. 2H and I). Therefore, we conducted a histopathological analysis of the lung tissues susceptible to injury in SAP. The lung histopathological sections of mice in the SAP-ALI group exhibited marked thickened alveolar septa, alveolar edema or collapse, vascular congestion, and the presence of immune cell infiltration within the lung tissue structure [41]. Conversely, the mSe-PP group displayed significant improvements (Fig. 3E and H). These results indicated that the biodistribution characteristics of mSe-PP support the possibility that mSe-PP may be a strategy for achieving dual targeting therapy for AP involving both the pancreas and lungs.

Furthermore, immunohistochemical staining of myeloperoxidase (MPO) was utilized to assess immune infiltration within the pancreatic parenchyma. The results revealed that, compared to SAP mice, the Se-PP and mSe-PP treatment groups exhibited lower neutrophil presence in the pancreatic tissue, especially in the group receiving intravenous mSe-PP (Fig. 3F and I). In line with these findings, the transcription levels of MCP-1, TNF-α, and IL-6, were significantly lower in pancreatic tissue of the mSe-PP-SAP group, demonstrating a substantial protective effect of mSe-PP during FAEE-SAP (Fig. 3J). Interestingly, we detected a marked attenuation of SAP-induced apoptosis in pancreatic acinar cells in the groups supplemented with Se-PP and mSe-PP, with mSe-PP showing a more pronounced effect, as confirmed by the reduction in TUNEL staining area (Fig. 3K and L). The results of the above experiments confirmed that mSe-PP treatment alleviated the severity of FAEE-SAP, mitigated the inflammation of pancreas and lungs, and reduced apoptosis of pancreatic acinar cells, whereas Se-PP was only effective in some of the inflammatory markers, thus the overall therapeutic efficacy was limited.

3.5. mSe-PP ameliorated pancreatic inflammatory cell infiltration in SAP

To further delve immune infiltration during the SAP period, a multichannel flow cytometry approach was employed to evaluate the infiltration of pancreatic innate immune cells, including neutrophils and macrophages. Supplementation of Se-PP and mSe-PP markedly reduced the number of $CD11b^+$ $Ly6G^+$ neutrophils in the pancreas following SAP induction, with mSe-PP supplementation achieving a greater reduction in infiltration levels (Fig. 4A and B). However Se-PP did not decreased pancreatic $CD11b^+$ $F4/80^+$ macrophages infiltration (Fig. 4C and D). Furthermore, we assessed immune infiltration of the pancreas by staining with CD45, a pan-leukocyte marker (Fig. 4E and F) and F4/80, a macrophage marker(Fig. 4G and H). Compared to the SAP group, mSe-PP group exhibited a marked decrease in the counts of $CD45^+$ and $F4/80^+$ cells, indicating a clear reduction in disease severity. These phenomena suggested that Se-PP and mSe-PP possess immunomodulatory effects on the pancreas, with mSe-PP demonstrating superior therapeutic efficacy over Se-PP.

3.6. mSe-PP reduced the severity of mild acute pancreatitis and decreased inflammatory infiltration

In mild acute pancreatitis, we induced pancreatitis using cerulein, as shown in Fig. S5B. Firstly, at 24 h into disease progression, the macroscopic morphology of the harvested pancreas showed edema following caerulein injection, which was alleviated after treatment, with mSe-PP demonstrating a more pronounced effect (Fig. S5D). We found that CAE-AP mice injected with mSe-PP exhibited significantly reduced levels of serum amylase, lipase, and pro-inflammatory cytokines including IL-6, TNF-α, and MCP-1, in contrast to both the AP and Se-PP-AP groups (Fig. 5A-C), indicating a systemic inhibitory effect on the development of AP.

Secondly, by histopathological analysis of the pancreas, we found CAE-AP mice displayed notable widening of the interlobular spaces, acinar cell necrosis, and inflammatory cell infiltration. In contrary, the pancreatic tissues of mSe-PP-AP mice closely resembled that of healthy mice, demonstrating significant pancreatic protection during AP (Fig. 5D and F). Furthermore, immunohistochemical staining of MPO, the transcription levels of inflammatory cytokines in pancreatic tissue and the number of apoptotic cells in pancreas sections were lower in the mSe-PP-AP than in the Se-PP-AP group (Fig. 5E, G-H and Figs. S5E and F).

During CAE-AP, supplementation with Se-PP and mSe-PP showed a similar trend to FAEE-SAP in terms of infiltrating neutrophils and macrophages(Fig. 5I, J and Figs. S5G–J). These results reaffirmed the systemic inhibitory and immunomodulatory effects of mSe-PP against AP.

Finally, the safety of each treatment was assessed upon completion of

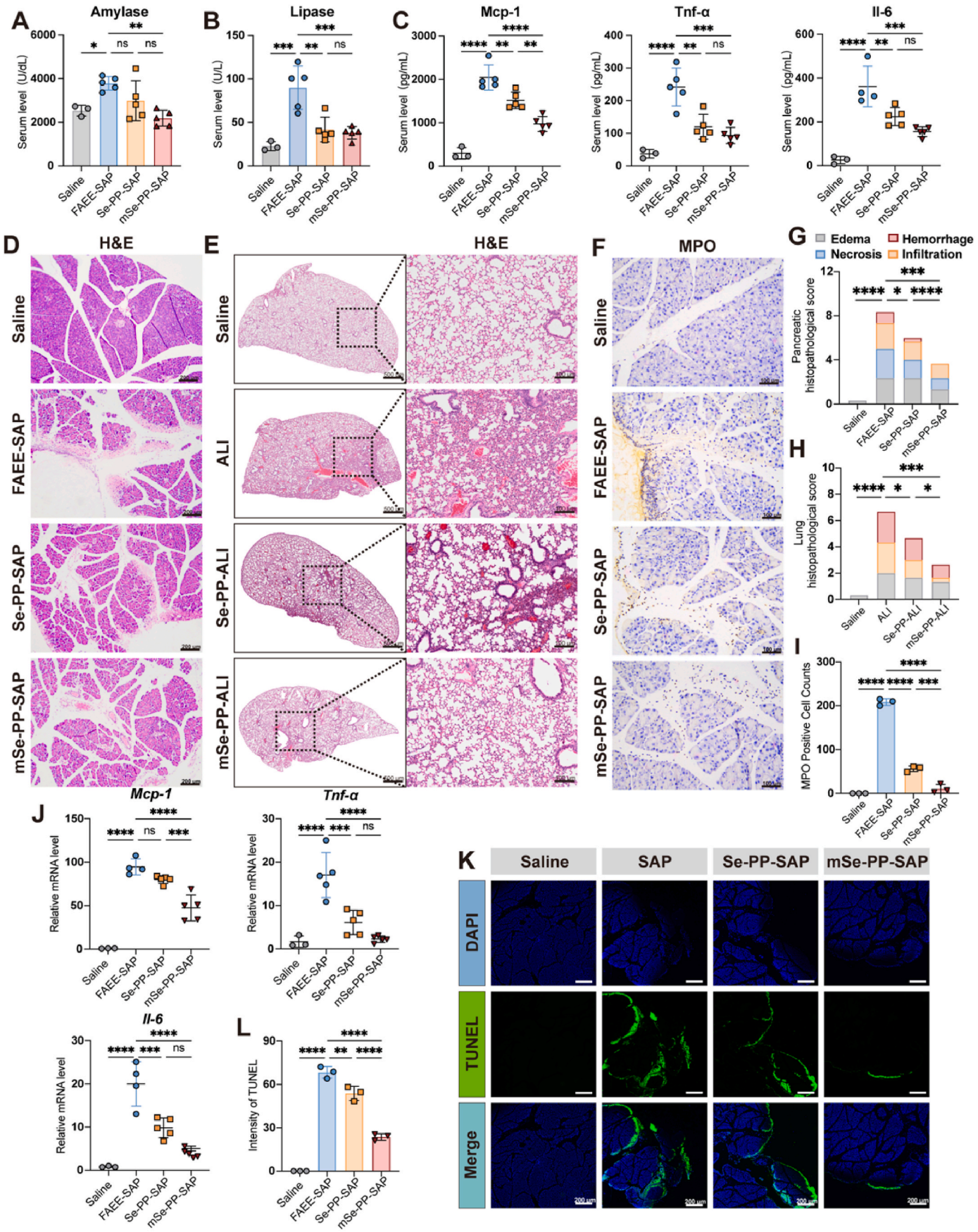

(caption on next page)

Fig. 3. mSe-PP alleviated the severity of fatty acid ethyl ester-induced SAP and reduced inflammation in the pancreas and lungs. (A, B) Amylase and lipase activity profile in serum of SAP mice treated with Se-PP and mSe-PP. (C) Concentration profiles of key inflammatory cytokines, including MCP-1, TNF-α, and IL-6, in the serum of SAP mice treated with different nanoparticle formulations. (D) Representative images of H&E staining on pancreas sections collected 12 h after receiving the treatments. Scale bars, 200 μm. (E) Representative H&E staining images and histology scores of lung tissues in different groups. Scale bars indicated 500 μm/100 μm. (F) Immunohistochemical staining of MPO representative images. Scale bars, 100 μm. (G) Total injury score in pancreas of FAEE-SAP in mice. (H) Histology scores of lung tissues in different groups. (I) The quantification of immunohistochemical staining for MPO. (J) Quantitative Real-time PCR results of MCP-1, TNF-α, and IL-6 in pancreas of different groups. (K) The quantitative evaluation by TUNEL fluorescence staining. (L) TUNEL fluorescence staining for evaluation of pancreatic apoptosis. Scale bars, 200 μm. Each dot represents a mouse (n = 3–5). ns P>0.05, *p < 0.05, **p < 0.01, ***p < 0.001 and ****P < 0.0001.

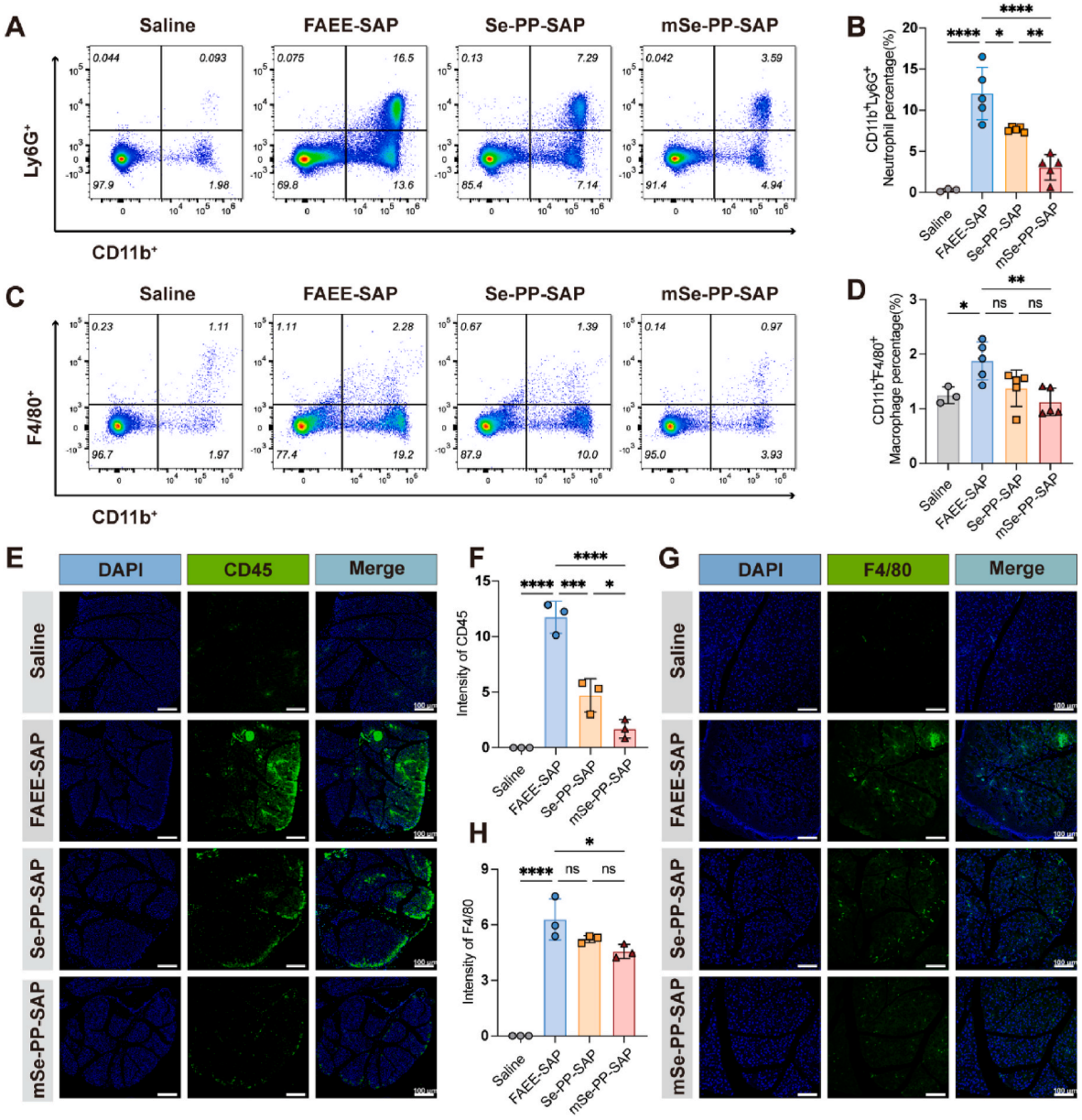

Fig. 4. mSe-PP ameliorated pancreatic inflammatory cell infiltration in fatty acid ethyl ester-induced SAP. (A-B, C-D) The frequencies of neutrophils ($CD11b^+$ $Ly6G^+$) and total macrophages ($CD11b^+$ $F4/80^+$) in the pancreas were detected by flow cytometry. Photomicrographs of (E) CD45 and (G) F4/80 immunofluorescence in the pancreas, Scale bars, 100 μm. (F, H) Quantitative evaluation of the intensities in CD45 and F4/80 fluorescence staining. Each dot represents a mouse (n = 3–5). ns P>0.05, *p < 0.05, **p < 0.01, ***p < 0.001 and ****P < 0.0001.

all administrations. No abnormalities were obsevered in hematological parameters (Figs. S6A–D), biomarkers of liver and kidney function (Figs. S6E–H) as well as H&E stained organ sections (Fig. S6I). These findings suggested that mSe-PP demonstrated excellent biocompatibility and minimal adverse effects.

3.7. The alleviation of AP by mSe-PP treatment was associated with the inhibition of the AKT/mTOR signaling and the mitigation of autophagic flux impairment

To explain the therapeutic mechanism of Se-PP and mSe-PP in AP mice, we investigated the relationships among mSe-PP, the AKT/mTOR signaling pathways and autophagy. During AP, the AKT/mTOR pathway

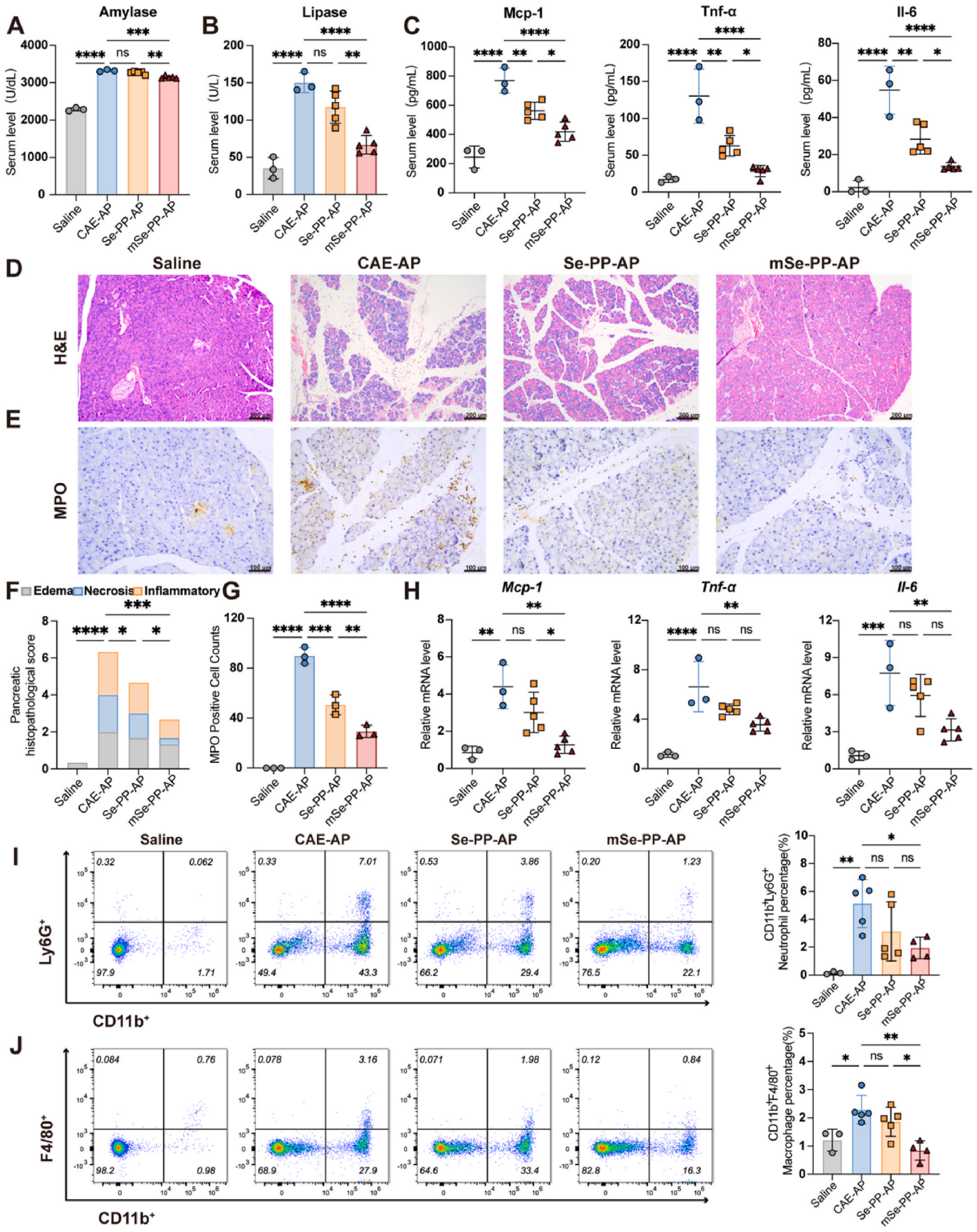

(caption on next page)

Fig. 5. mSe-PP reduced the severity of caerulein-induced acute pancreatitis and decreased inflammatory infiltration. (A, B) Serum levels of amylase and lipase after treated with Se-PP and mSe-PP. (C) Concentration profiles of key inflammatory cytokines, including MCP-1, TNF-α, and IL-6, in the serum of AP mice treated with different nanoparticle formulations. (D) Histopathological changes of pancreatic samples observed by H&E staining. Scale bars, 200 μm. (E) Immunohistochemical staining of MPO representative images. Scale bars, 100 μm. (F) Total injury score in pancreas of caerulein-induced acute pancreatitis in mice. (G) The quantification of immunohistochemical staining for MPO. (H) Quantitative Real-time PCR results of MCP-1, TNF-α, and IL-6 in pancreas of different groups. (I) The frequencies of neutrophils ($CD11b^+$ $Ly6G^+$) and (J) total macrophages ($CD11b^+$ $F4/80^+$) in the pancreas were detected by flow cytometry. Each dot represents a mouse (n = 3–5). ns $P>0.05$, *$p < 0.05$, **$p < 0.01$, ***$p < 0.001$ and ****$P < 0.0001$.

was activated, leading to impaired autophagy, as evidenced by increased levels of autophagy markers such as p62 and LC3 (Fig. 6A–D). However, mSe-PP administration reduced impaired autophagic flux, with the inhibition of AKT/mTOR signaling.

Alternatively, we examined AKT p62 and LC3 by an immunofluorescence assay. The corresponding immunofluorescence results agreed with what western blot had confirmed, showing that mSe-PP alleviates impaired autophagy in AP and SAP through inhibition of AKT/mTOR signaling (Fig. 6E and F).

3.8. mSe-PP inhibited the AKT/mTOR signalling pathway, restored impaired autophagy, and attenuated inflammatory responses, apoptosis and oxidative stress in RAW264.7 cells

Given the essential factor of macrophages in the pathogenesis of AP and the macrophage-targeting properties of mSe-PP [46–48]. We used RAW264.7 cells as the central cell model in this study (Fig. 7A). Cell proliferation experiments showed that mSe-PP did not show toxic effects of inhibiting cell proliferation, even at high concentrations of 0.48 mg/mL, whereas Se-PP demonstrated cytotoxicity at this concentration (Fig. 7B). Enzyme-linked immunosorbent assay (ELISA) experiments revealed that mSe-PP significantly reduced the secretion levels of MCP-1, IL-6, and TNF-α in LPS-stimulated RAW264.7 cells compared to Se-PP (Fig. 7C). Gene expression analysis of MCP-1, IL-1β, and CXCL2, in RAW264.7 cells also revealed similar changes (Fig. 7D).

Various damage-associated molecular patterns (DAMPs) can stimulate macrophages infiltrated at anatomical sites, leading to elevated levels of ROS which in turn triggers phenotypic switching and cell death of macrophages infiltrated in the pancreas [49]. As depicted in Fig. 6E and F, mSe-PP's anti-inflammatory treatment significantly reduced the intracellular ROS levels in macrophages compared to LPS-induced oxidative damage and excessive ROS generation. Furthermore, there was no doubt that the number of apoptotic and necrotic cells was substantially increased after LPS incubation, compared to the control group. After co-culturing with Se-PP and mSe-PP, cell apoptosis was mitigated, especially in the mSe-PP group (Fig. 6G and H). Together, these findings indicated that mSe-PP provided superior protection to cells against oxidative damage compared to Se-PP. In summary, mSe-PP can serve as an immunosuppressive and immunomodulatory agent against cell inflammation and oxidative stress.

To determine the influence of Se-PP and mSe-PP treatment on the AKT/mTOR signaling pathways and autophagy in RAW264.7 cells, we examined the expression of key proteins in the AKT/mTOR pathway and autophagy-related proteins. The western blot results indicated that during RAW264.7 cells activation, AKT/mTOR signaling pathway was activated and cellular autophagy was impaired, leading to p62 and LC3 accumulation. However, both Se-PP and mSe-PP can restore the impaired autophagy, with mSe-PP being particularly effective in restoring cellular autophagy levels (Fig. 6I). Immunofluorescence staining revealed that the LPS-treated group exhibited elevated LC3 levels, while the Se-PP and mSe-PP treatment groups showed reductions, especially in the mSe-PP-LPS group (Fig. 6J).

4. Discussion

AP currently lacks therapeutic agents capable of altering the course of the disease. Preliminary studies have revealed that selenylated polysaccharides exhibit dual functionalities. Firstly, they retain the active hydroxyl groups of polysaccharides, and secondly, they endow the material with selenium's physiological properties, such as antitumor activity [50], antioxidant characteristics [51], and immunomodulatory effects [33]. By leveraging the abundant functional groups in selenopolysaccharides as an ideal template for nanoparticle synthesis [40], the functional modification of selenium can further enhance its applicability in multimodal therapeutic strategies [50]. Therefore, selenylated polysaccharides can inhibit inflammatory pathways within cells at inflammatory sites in inflammatory diseases [21,39,52]. However, the potential of selenylated Poria cocos polysaccharides as a therapeutic agent for treating AP remains undetermined. In this experimental investigation, we demonstrated that Se-P exhibited therapeutic potential for AP; however, similar to challenges encountered in the development of AP treatments, it demonstrated limited efficacy, poor bioavailability, and a lack of selectivity.

In recent years, precision treatment of AP under nanotherapeutic platforms has been gradually explored, and a variety of drugs and methods targeting the inflammatory microenvironment as well as the pathophysiology of AP have emerged [53,54], whereas cell membrane encapsulation, as a camouflage strategy, not only circumvents the MPS, but also confers nanoparticles with inflammatory recruitment and precision targeting capabilities. This study introduced a macrophage-mimicking targeting approach using membrane camouflage. We hypothesized that emulating the natural recruitment of macrophages to sites of inflammation during the progression of AP could facilitate the precise delivery of anti-inflammatory therapies. In our study, there was increased accumulation of macrophage membrane-camouflaged liposomes in the pancreas and lungs of mice with AP, which could be attributed to various reasons. For instance, nano-drug delivery systems of certain sizes can selectively accumulate at inflammatory sites through extravasation from leaky vessels and subsequent isolation mediated by inflammatory cells (ELVIS) [55]. Additionally, macrophage membrane camouflage may enhance active homing to inflamed lesions, simulating the natural process of immune cell aggregation during the progression of AP. This homing effect enabled macrophage membrane-camouflaged liposomal materials to exhibit therapeutic effects far superior to unencapsulated selenylated polysaccharides, both in severe acute and mild acute pancreatitis.

AKT is a serine/threonine kinase that is activated intracellularly, with phosphorylated AKT (p-AKT) being its activated form. mTOR is a major intracellular autophagy inhibitor, and activation of mTOR through phosphorylation (p-mTOR) is indicative of its activation by p-AKT [56–58]. Autophagy is a crucial mechanism for maintaining cellular homeostasis in eukaryotic cells [59]. Therefore, modulating autophagy processes to treat AP is a potential strategy and prospect in drug development. Many selenylated polysaccharides have been shown to exert pharmacological effects by modulating autophagy through the PI3K/AKT/mTOR pathway [13,14]. Thus, we speculated that the alleviating effects of Se-PP and mSe-PP on AP may require modulation of autophagy mediated by the AKT/mTOR pathway. Our results found that mSe-PP restored impaired autophagic flux, inhibited the AKT/mTOR signaling pathway, and maintained cellular homeostasis.

This study demonstrated that macrophages were potential cell membrane donors that can optimize the pharmacokinetics and safety of drugs. Macrophage membrane camouflage technology is expected to be translated into clinical trials and holds promise in the biomedical field [6,55,60]. However, some limitations were found in our research. In vitro cell uptake experiments revealed that after macrophage membrane

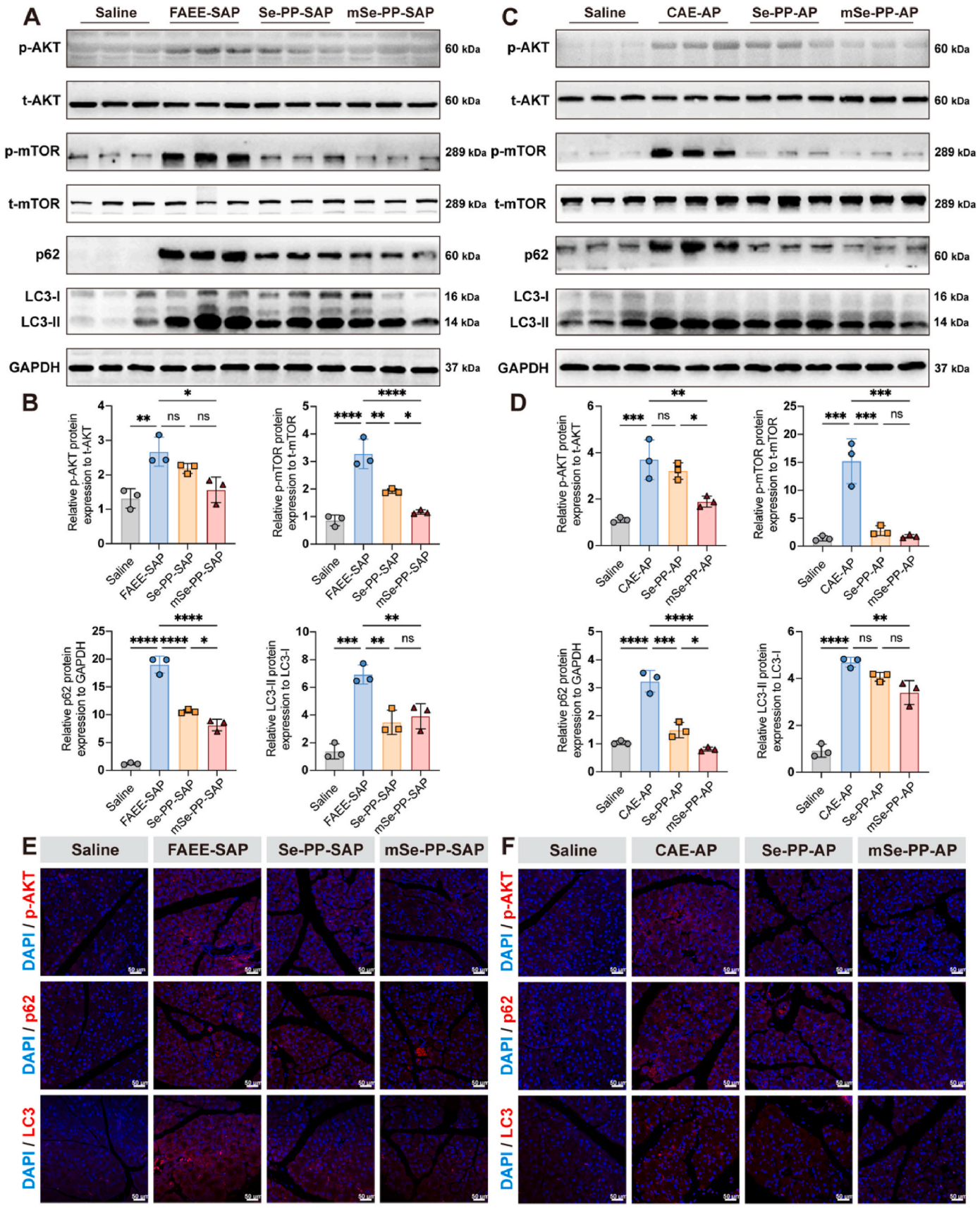

Fig. 6. mSe-PP downregulated proteins in the AKT/mTOR pathway and reduced autophagic flux impairment in the pancreas. Western blot results and analysis of AKT, p-AKT, mTOR, p-mTOR, p62, and LC3 in the FAEE-SAP (A, B) and CAE-AP (C, D) models respectively. p-AKT versus AKT, p-mTOR versus mTOR, p62 versus GAPDH, LC3-II versus LC3-I. Immunofluorescence staining for p-AKT, p62 and LC3 in the FAEE-SAP (E) and CAE-AP (F) models. Scale bars, 50 μm. Each dot represents a mouse (n = 3–5). ns P>0.05, *p < 0.05, **p < 0.01, ***p < 0.001 and ****P < 0.0001.

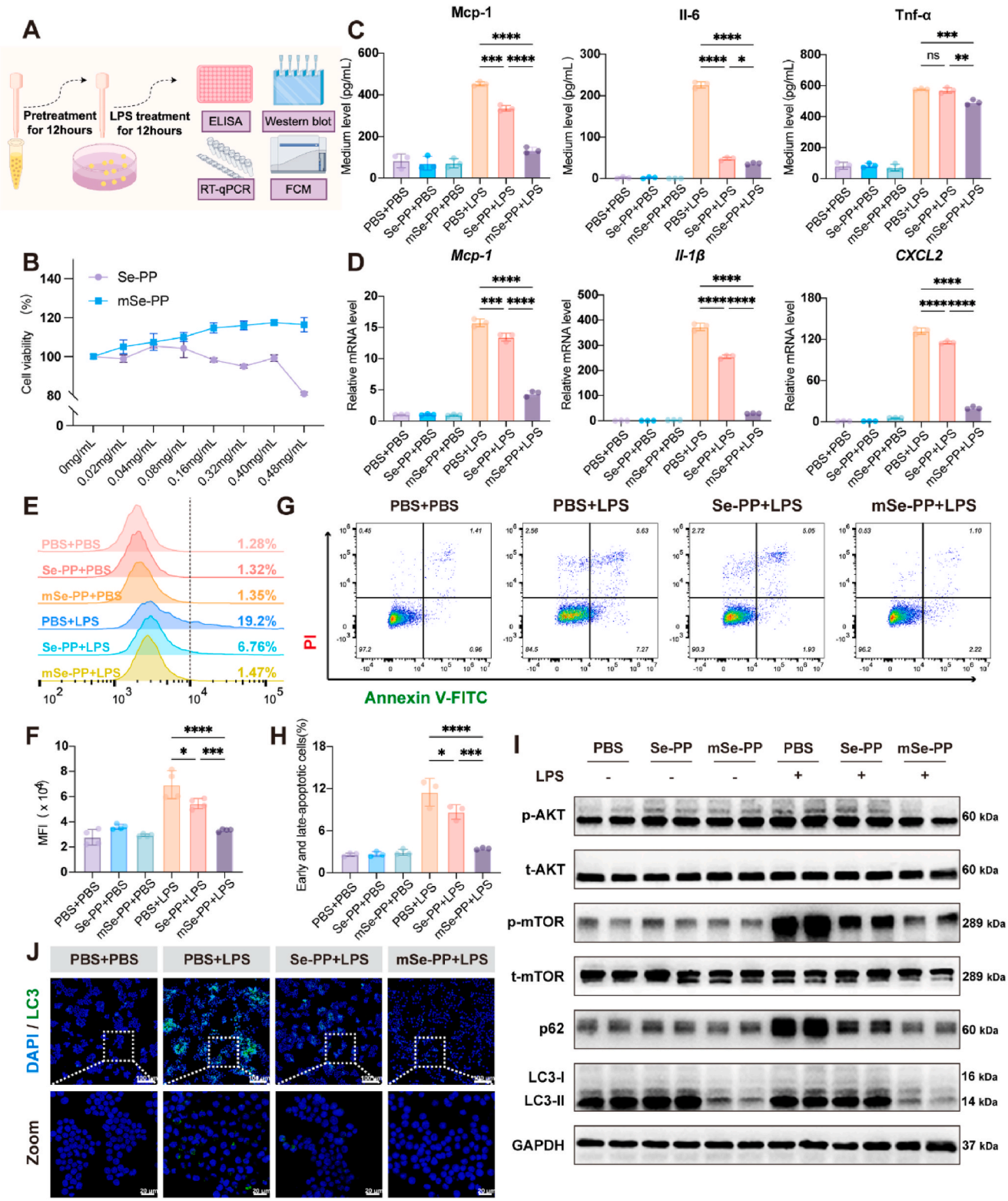

Fig. 7. mSe-PP inhibited the AKT/mTOR signaling pathway to restore impaired autophagy, alleviating inflammation, apoptosis and oxidative stress in RAW264.7 cells. (A) Overall experimental procedure. RAW264.7 cells were pretreated with Se-PP and mSe-PP for 12 h, followed by stimulation with PBS or LPS for 12 h. Subsequently, the collected cells were subjected to enzyme-linked immunosorbent assay (ELISA), reverse transcription quantitative polymerase chain reaction (RT-qPCR), western blot, and flow cytometry analyses. (B) The cytotoxicity of different concentrations of Se-PP and mSe-PP nanoparticles on RAW264.7 cells measured by CCK8 assay. (C) The alterations in inflammatory factors, including MCP-1, TNF-α, and IL-6, in the medium supernatant following treatment with Se-PP and mSe-PP. (D) Quantitative Real-time PCR results of MCP-1, IL-1β, and CXCL2 in RAW264.7 cells from different groups. (E, F) Flow cytometry histogram and MFI after lipopolysaccharide treatment stained with DCFH-DA. MFI, mean fluorescence intensity. (G, H) Apoptosis of RAW264.7 cells after drug treatment was detected by staining with Annexin V-FITC/PI and flow cytometry analysis. (I) Western blot results of AKT, p-AKT, mTOR, p-mTOR, p62, and LC3 in RAW264.7 cells. (J) Immunofluorescence staining for LC3. Scale bars indicated 100 μm/20 μm. Each dot represents a sample (n = 3). ns $P>0.05$, *$p < 0.05$, **$p < 0.01$, ***$p < 0.001$ and ****$P < 0.0001$.

encapsulation, activated macrophages and endothelial cells exhibited reduced uptake of nanoparticles, which may be associated with the negatively charged nature of macrophage membranes. Although macrophage biomimetic nanoparticles had largely alleviated AP, they can still be optimized. Before application in clinical trials, the biological safety of cell membranes should be carefully studied [38]. Although our experiments confirmed good biocompatibility through evaluation of organ histopathology and liver and kidney function, more reliable and direct evidence should be obtained from prospective clinical studies to further refine experimental research and optimize and evaluate the anti-inflammatory properties and biosafety of macrophage biomimetic selenium polysaccharide nanoparticles.

5. Conclusion

This study highlights a promising approach that could pave the way for the advancement of dual-targeted nanotherapy for AP, addressing both the pancreas and lungs. Se-P exhibited anti-inflammatory and antioxidant effects, but their stability and non-selective tissue distribution may hinder their efficacy. Modification of macrophage membrane biomimetics on Se-P can enhance the homing capability of liposomes to AP lesions and achieve targeted action against innate inflammatory chemotaxis, thereby reducing non-specific tissue distribution. Results indicated that due to the aggregation effect of mSe-PP in pancreatic tissue, compared to uncoated nanoparticles, mSe-PP can more effectively inhibited systemic inflammation, acinar cell apoptosis, and infiltration of innate immune cells in both mild and severe AP. In RAW264.7 cells, macrophage-mimicking nanoparticles more effectively restored impaired autophagic flux by inhibiting activation of the AKT/mTOR pathway, thereby alleviating inflammation, cell apoptosis, and oxidative stress. This design established a nanoplatform comprising selenium polysaccharides and macrophage mimicry technology, offering an innovative approach for the clinical management of AP with inflammation chemotactic properties and anti-inflammatory antioxidant effects mimicking macrophage biology behaviors.

CRediT authorship contribution statement

Fengyu Shi: Writing – original draft, Investigation, Conceptualization. **Akmal Ergashev:** Visualization, Methodology. **Zhenyan Pan:** Resources. **Hongwei Sun:** Validation, Investigation. **Lingming Kong:** Formal analysis. **Yuepeng Jin:** Formal analysis. **Tan Zhang:** Visualization, Methodology. **Zhu Liu:** Resources. **Haonan Xie:** Data curation. **Jinhui Wang:** Data curation. **Huiping Li:** Supervision. **Yi Wang:** Supervision. **Lifei Zheng:** Project administration. **Jianliang Shen:** Project administration. **Andreas Herrmann:** Writing – review & editing, Funding acquisition, Conceptualization. **Gang Chen:** Writing – review & editing, Funding acquisition, Conceptualization. **Hongru Kong:** Writing – review & editing, Funding acquisition, Conceptualization.

Funding sources

This work was supported by the Wenzhou Science & Technology Bureau project [grant number Y20180103] and the Zhejiang Provincial Natural Science Foundation [grant number LY20H150005].

Declaration of competing interest

The authors declare the following financial interests/personal relationships which may be considered as potential competing interests: Hongru Kong reports financial support was provided by Wenzhou Municipal Science and Technology Bureau. Huiping Li reports financial support was provided by Zhejiang Province Natural Science Foundation. If there are other authors, they declare that they have no known competing financial interests or personal relationships that could have appeared to influence the work reported in this paper.

Appendix A. Supplementary data

Supplementary data to this article can be found online at https://doi.org/10.1016/j.mtbio.2024.101406.

Data availability

Data will be made available on request.

References

[1] P.J. Lee, G.I. Papachristou, New insights into acute pancreatitis, Nat. Rev. Gastroenterol. Hepatol. 16 (8) (2019) 479–496, https://doi.org/10.1038/s41575-019-0158-2.
[2] P. Xie, L. Zhang, H. Shen, H. Wu, J. Zhao, S. Wang, L. Hu, Biodegradable MoSe(2)-polyvinylpyrrolidone nanoparticles with multi-enzyme activity for ameliorating acute pancreatitis, J. Nanobiotechnol. 20 (1) (2022) 113, https://doi.org/10.1186/s12951-022-01288-x.
[3] E. Afghani, S.J. Pandol, T. Shimosegawa, R. Sutton, B.U. Wu, S.S. Vege, F. Gorelick, M. Hirota, J. Windsor, S.K. Lo, M.L. Freeman, M.M. Lerch, Y. Tsuji, G.Y. Melmed, W. Wassef, J. Mayerle, Acute pancreatitis-progress and challenges: a report on an international symposium, Pancreas 44 (8) (2015) 1195–1210, https://doi.org/10.1097/mpa.0000000000000500.
[4] N.J. Schepers, O.J. Bakker, M.G. Besselink, U. Ahmed Ali, T.L. Bollen, H. G. Gooszen, H.C. van Santvoort, M.J. Bruno, Impact of characteristics of organ failure and infected necrosis on mortality in necrotising pancreatitis, Gut 68 (6) (2019) 1044–1051, https://doi.org/10.1136/gutjnl-2017-314657.
[5] P.K. Garg, V.P. Singh, Organ failure due to systemic injury in acute pancreatitis, Gastroenterology 156 (7) (2019) 2008–2023, https://doi.org/10.1053/j.gastro.2018.12.041.
[6] Q. Zhang, J. Zhou, J. Zhou, R.H. Fang, W. Gao, L. Zhang, Lure-and-kill macrophage nanoparticles alleviate the severity of experimental acute pancreatitis, Nat. Commun. 12 (1) (2021) 4136, https://doi.org/10.1038/s41467-021-24447-4.
[7] IAP/APA evidence-based guidelines for the management of acute pancreatitis, Pancreatology 13 (4 Suppl 2) (2013) e1–e15, https://doi.org/10.1016/j.pan.2013.07.063.
[8] L. Boxhoorn, R.P. Voermans, S.A. Bouwense, M.J. Bruno, R.C. Verdonk, M. A. Boermeester, H.C. van Santvoort, M.G. Besselink, Acute pancreatitis, Lancet 396 (10252) (2020) 726–734, https://doi.org/10.1016/s0140-6736(20)31310-6.
[9] G. Biczo, E.T. Vegh, N. Shalbueva, O.A. Mareninova, J. Elperin, E. Lotshaw, S. Gretler, A. Lugea, S.R. Malla, D. Dawson, P. Ruchala, J. Whitelegge, S.W. French, L. Wen, S.Z. Husain, F.S. Gorelick, P. Hegyi, Z. Rakonczay Jr., I. Gukovsky, A. S. Gukovskaya, Mitochondrial dysfunction, through impaired autophagy, leads to endoplasmic reticulum stress, deregulated lipid metabolism, and pancreatitis in animal models, Gastroenterology 154 (3) (2018) 689–703, https://doi.org/10.1053/j.gastro.2017.10.012.
[10] I. Gukovsky, N. Li, J. Todoric, A. Gukovskaya, M. Karin, Inflammation, autophagy, and obesity: common features in the pathogenesis of pancreatitis and pancreatic cancer, Gastroenterology 144 (6) (2013), https://doi.org/10.1053/j.gastro.2013.02.007, 1199-209.e4.
[11] X. Ouyang, Z. He, H. Fang, H. Zhang, Q. Yin, L. Hu, F. Gao, H. Yin, T. Hao, Y. Hou, Q. Wu, J. Deng, J. Xu, Y. Wang, C. Chen, A protein encoded by circular ZNF609 RNA induces acute kidney injury by activating the AKT/mTOR-autophagy pathway, Mol. Ther. 31 (6) (2023) 1722–1738, https://doi.org/10.1016/j.ymthe.2022.09.007.
[12] W. Zheng, W. Xie, D. Yin, R. Luo, M. Liu, F. Guo, ATG5 and ATG7 induced autophagy interplays with UPR via PERK signaling, Cell Commun. Signal. 17 (1) (2019) 42, https://doi.org/10.1186/s12964-019-0353-3.
[13] D. Liu, J. Xu, G. Qian, M. Hamid, F. Gan, X. Chen, K. Huang, Selenizing astragalus polysaccharide attenuates PCV2 replication promotion caused by oxidative stress through autophagy inhibition via PI3K/AKT activation, Int. J. Biol. Macromol. 108 (2018) 350–359, https://doi.org/10.1016/j.ijbiomac.2017.12.010.
[14] Y. Tan, L. Yin, Z. Sun, S. Shao, W. Chen, X. Man, Y. Du, Y. Chen, Astragalus polysaccharide exerts anti-Parkinson via activating the PI3K/AKT/mTOR pathway to increase cellular autophagy level in vitro, Int. J. Biol. Macromol. 153 (2020) 349–356, https://doi.org/10.1016/j.ijbiomac.2020.02.282.
[15] V. Panwar, A. Singh, M. Bhatt, R.K. Tonk, S. Azizov, A.S. Raza, S. Sengupta, D. Kumar, M. Garg, Multifaceted role of mTOR (mammalian target of rapamycin) signaling pathway in human health and disease, Signal Transduct. Targeted Ther. 8 (1) (2023) 375, https://doi.org/10.1038/s41392-023-01608-z.
[16] Y. Duan, J. Huang, M. Sun, Y. Jiang, S. Wang, L. Wang, N. Yu, D. Peng, Y. Wang, W. Chen, Y. Zhang, Poria cocos polysaccharide improves intestinal barrier function and maintains intestinal homeostasis in mice, Int. J. Biol. Macromol. 249 (2023) 125953, https://doi.org/10.1016/j.ijbiomac.2023.125953.
[17] T. Xu, H. Zhang, S. Wang, Z. Xiang, H. Kong, Q. Xue, M. He, X. Yu, Y. Li, D. Sun, P. Gao, Z. Cong, A review on the advances in the extraction methods and structure elucidation of Poria cocos polysaccharide and its pharmacological activities and drug carrier applications, Int. J. Biol. Macromol. 217 (2022) 536–551, https://doi.org/10.1016/j.ijbiomac.2022.07.070.
[18] S. Zhang, H. Zhang, L. Shi, Y. Li, M. Tuerhong, M. Abudukeremu, J. Cui, Y. Li, D. Q. Jin, J. Xu, Y. Guo, Structure features, selenylation modification, and improved anti-tumor activity of a polysaccharide from Eriobotrya japonica, Carbohydr. Polym. 273 (2021) 118496, https://doi.org/10.1016/j.carbpol.2021.118496.

[19] Z. Gao, C. Zhang, W. Tian, K. Liu, R. Hou, C. Yue, Y. Wu, D. Wang, J. Liu, Y. Hu, Y. Yang, The antioxidative and hepatoprotective effects comparison of Chinese angelica polysaccharide(CAP)and selenizing CAP (sCAP) in CCl(4) induced hepatic injury mice, Int. J. Biol. Macromol. 97 (2017) 46–54, https://doi.org/10.1016/j.ijbiomac.2017.01.013.
[20] F. Huang, X.Y. Sun, J.M. Ouyang, Preparation and characterization of selenized Astragalus polysaccharide and its inhibitory effect on kidney stones, Mater. Sci. Eng., C 110 (2020) 110732, https://doi.org/10.1016/j.msec.2020.110732.
[21] Y. Xu, X.C. Wang, W. Jiang, L.H. Chen, T. Chen, D. Wu, J.N. Hu, Porphyra haitanensis polysaccharide-functionalized selenium nanoparticles for effective alleviation of ulcerative colitis, Int. J. Biol. Macromol. 253 (Pt 8) (2023) 127570, https://doi.org/10.1016/j.ijbiomac.2023.127570.
[22] H. Wang, Y. Li, X. Wang, Y. Li, J. Cui, D.Q. Jin, M. Tuerhong, M. Abudukeremu, J. Xu, Y. Guo, Preparation and structural properties of selenium modified heteropolysaccharide from the fruits of Akebia quinata and in vitro and in vivo antitumor activity, Carbohydr. Polym. 278 (2022) 118950, https://doi.org/10.1016/j.carbpol.2021.118950.
[23] L. Wang, X. Li, B. Wang, Synthesis, characterization and antioxidant activity of selenium modified polysaccharides from Hohenbuehelia serotina, Int. J. Biol. Macromol. 120 (Pt B) (2018) 1362–1368, https://doi.org/10.1016/j.ijbiomac.2018.09.139.
[24] R. Hou, J. Chen, C. Yue, X. Li, J. Liu, Z. Gao, C. Liu, Y. Lu, D. Wang, H. Li, Y. Hu, Modification of lily polysaccharide by selenylation and the immune-enhancing activity, Carbohydr. Polym. 142 (2016) 73–81, https://doi.org/10.1016/j.carbpol.2016.01.032.
[25] Y. Liu, Y. You, Y. Li, L. Zhang, L. Yin, Y. Shen, C. Li, H. Chen, S. Chen, B. Hu, D. Chen, The characterization, selenylation and antidiabetic activity of mycelial polysaccharides from Catathelasma ventricosum, Carbohydr. Polym. 174 (2017) 72–81, https://doi.org/10.1016/j.carbpol.2017.06.050.
[26] Z. Gao, K. Liu, W. Tian, H. Wang, Z. Liu, Y. Li, E. Li, C. Liu, X. Li, R. Hou, C. Yue, D. Wang, Y. Hu, Effects of selenizing angelica polysaccharide and selenizing garlic polysaccharide on immune function of murine peritoneal macrophage, Int. Immunopharm. 27 (1) (2015) 104–109, https://doi.org/10.1016/j.intimp.2015.04.052.
[27] H. Li, H. Che, J. Xie, X. Dong, L. Song, W. Xie, J. Sun, Supplementary selenium in the form of selenylation α-D-1,6-glucan ameliorates dextran sulfate sodium induced colitis in vivo, Int. J. Biol. Macromol. 195 (2022) 67–74, https://doi.org/10.1016/j.ijbiomac.2021.11.189.
[28] F. Liu, Y. Liu, X. Feng, S.A. Ibrahim, W. Huang, Structure characterization and in vitro immunomodulatory activities of carboxymethyl pachymaran, Int. J. Biol. Macromol. 178 (2021) 94–103, https://doi.org/10.1016/j.ijbiomac.2021.02.046.
[29] L. Cheng, Y. Wang, X. He, X. Wei, Preparation, structural characterization and bioactivities of Se-containing polysaccharide: a review, Int. J. Biol. Macromol. 120 (Pt A) (2018) 82–92, https://doi.org/10.1016/j.ijbiomac.2018.07.106.
[30] J. Cheng, R. Zhang, C. Li, H. Tao, Y. Dou, Y. Wang, H. Hu, J. Zhang, A targeting nanotherapy for abdominal aortic aneurysms, J. Am. Coll. Cardiol. 72 (21) (2018) 2591–2605, https://doi.org/10.1016/j.jacc.2018.08.2188.
[31] Y. Dou, C. Li, L. Li, J. Guo, J. Zhang, Bioresponsive drug delivery systems for the treatment of inflammatory diseases, J. Contr. Release 327 (2020) 641–666, https://doi.org/10.1016/j.jconrel.2020.09.008.
[32] I. Armenia, C. Cuestas Ayllón, B. Torres Herrero, F. Bussolari, G. Alfranca, V. Grazú, J. Martínez de la Fuente, Photonic and magnetic materials for on-demand local drug delivery, Adv. Drug Deliv. Rev. 191 (2022) 114584, https://doi.org/10.1016/j.addr.2022.114584.
[33] C. Ding, C. Yang, T. Cheng, X. Wang, Q. Wang, R. He, S. Sang, K. Zhu, D. Xu, J. Wang, X. Liu, X. Zhang, Macrophage-biomimetic porous Se@SiO(2) nanocomposites for dual modal immunotherapy against inflammatory osteolysis, J. Nanobiotechnol. 19 (1) (2021) 382, https://doi.org/10.1186/s12951-021-01128-4.
[34] M. Park, H.J. Oh, J. Han, S.H. Hong, W. Park, H. Song, Liposome-mediated small RNA delivery to convert the macrophage polarity: a novel therapeutic approach to treat inflammatory uterine disease, Mol. Ther. Nucleic Acids 30 (2022) 663–676, https://doi.org/10.1016/j.omtn.2022.11.018.
[35] K. Jin, Z. Luo, B. Zhang, Z. Pang, Biomimetic nanoparticles for inflammation targeting, Acta Pharm. Sin. B 8 (1) (2018) 23–33, https://doi.org/10.1016/j.apsb.2017.12.002.
[36] J. Cai, H. Tao, H. Liu, Y. Hu, S. Han, W. Pu, L. Li, G. Li, C. Li, J. Zhang, Intrinsically bioactive and biomimetic nanoparticle-derived therapies alleviate asthma by regulating multiple pathological cells, Bioact. Mater. 28 (2023) 12–26, https://doi.org/10.1016/j.bioactmat.2023.04.023.
[37] F. Hu, N. Lou, J. Jiao, F. Guo, H. Xiang, D. Shang, Macrophages in pancreatitis: mechanisms and therapeutic potential, Biomed. Pharmacother. 131 (2020) 110693, https://doi.org/10.1016/j.biopha.2020.110693.
[38] K. Ying, Y. Zhu, J. Wan, C. Zhan, Y. Wang, B. Xie, P. Xu, H. Pan, H. Wang, Macrophage membrane-biomimetic adhesive polycaprolactone nanocamptothecin for improving cancer-targeting efficiency and impairing metastasis, Bioact. Mater. 20 (2023) 449–462, https://doi.org/10.1016/j.bioactmat.2022.06.013.
[39] R. Ye, Q. Guo, J. Huang, Z. Wang, Y. Chen, Y. Dong, Eucommia ulmoides polysaccharide modified nano-selenium effectively alleviated DSS-induced colitis through enhancing intestinal mucosal barrier function and antioxidant capacity, J. Nanobiotechnol. 21 (1) (2023) 222, https://doi.org/10.1186/s12951-023-01965-5.
[40] X.D. Shi, Y.Q. Tian, J.L. Wu, S.Y. Wang, Synthesis, characterization, and biological activity of selenium nanoparticles conjugated with polysaccharides, Crit. Rev. Food Sci. Nutr. 61 (13) (2021) 2225–2236, https://doi.org/10.1080/10408398.2020.1774497.
[41] L. Kong, J. Deng, X. Zhou, B. Cai, B. Zhang, X. Chen, Z. Chen, W. Wang, Sitagliptin activates the p62-Keap1-Nrf2 signalling pathway to alleviate oxidative stress and excessive autophagy in severe acute pancreatitis-related acute lung injury, Cell Death Dis. 12 (10) (2021) 928, https://doi.org/10.1038/s41419-021-04227-0.
[42] J. Liu, Z. Wu, Y. Liu, Z. Zhan, L. Yang, C. Wang, Q. Jiang, H. Ran, P. Li, Z. Wang, ROS-responsive liposomes as an inhaled drug delivery nanoplatform for idiopathic pulmonary fibrosis treatment via Nrf2 signaling, J. Nanobiotechnol. 20 (1) (2022) 213, https://doi.org/10.1186/s12951-022-01435-4.
[43] Y. Ma, L. Liu, B. Li, W. Wang, T. Zhao, Cdk2 suppresses IL-23 expression and the onset of severe acute pancreatitis, Immun Inflamm Dis 10 (6) (2022) e631, https://doi.org/10.1002/iid3.631.
[44] T. Bian, H. Li, Q. Zhou, C. Ni, Y. Zhang, F. Yan, Human β-Defensin 3 reduces TNF-α-induced inflammation and monocyte adhesion in human Umbilical Vein endothelial cells, Mediat. Inflamm. 2017 (2017) 8529542, https://doi.org/10.1155/2017/8529542.
[45] X. Liu, W. Luo, J. Chen, C. Hu, R.N. Mutsinze, X. Wang, Y. Zhang, L. Huang, W. Zuo, G. Liang, Y. Wang, USP25 Deficiency Exacerbates acute pancreatitis via up-regulating TBK1-NF-κB signaling in macrophages, Cell Mol Gastroenterol Hepatol 14 (5) (2022) 1103–1122, https://doi.org/10.1016/j.jcmgh.2022.07.013.
[46] R. Kang, M.T. Lotze, H.J. Zeh, T.R. Billiar, D. Tang, Cell death and DAMPs in acute pancreatitis, Mol. Med. 20 (1) (2014) 466–477, https://doi.org/10.2119/molmed.2014.00117.
[47] R. Hoque, M. Sohail, A. Malik, S. Sarwar, Y. Luo, A. Shah, F. Barrat, R. Flavell, F. Gorelick, S. Husain, W. Mehal, TLR9 and the NLRP3 inflammasome link acinar cell death with inflammation in acute pancreatitis, Gastroenterology 141 (1) (2011) 358–369, https://doi.org/10.1053/j.gastro.2011.03.041.
[48] Q. Zhao, Y. Wei, S.J. Pandol, L. Li, A. Habtezion, STING signaling promotes inflammation in experimental acute pancreatitis, Gastroenterology 154 (6) (2018) 1822–1835.e2, https://doi.org/10.1053/j.gastro.2018.01.065.
[49] A. Habtezion, A.S. Gukovskaya, S.J. Pandol, Acute pancreatitis: a Multifaceted Set of Organelle and cellular Interactions, Gastroenterology 156 (7) (2019) 1941–1950, https://doi.org/10.1053/j.gastro.2018.11.082.
[50] X. Liu, Y. Wang, Q. Yu, G. Deng, Q. Wang, X. Ma, Q. Wang, J. Lu, Selenium nanocomposites as multifunctional nanoplatform for imaging guiding synergistic chemo-photothermal therapy, Colloids Surf. B Biointerfaces 166 (2018) 161–169, https://doi.org/10.1016/j.colsurfb.2018.03.018.
[51] Z. Zheng, L. Liu, K. Zhou, L. Ding, J. Zeng, W. Zhang, Anti-oxidant and anti-endothelial dysfunctional properties of nano-selenium in vitro and in vivo of Hyperhomocysteinemic rats, Int. J. Nanomed. 15 (2020) 4501–4521, https://doi.org/10.2147/ijn.S255392.
[52] R. Bo, X. Ji, H. Yang, M. Liu, J. Li, The characterization of optimal selenized garlic polysaccharides and its immune and antioxidant activity in chickens, Int. J. Biol. Macromol. 182 (2021) 136–143, https://doi.org/10.1016/j.ijbiomac.2021.03.197.
[53] Y. Wang, D. Qian, X. Wang, X. Zhang, Z. Li, X. Meng, L. Yu, X. Yan, Z. He, Biomimetic Trypsin-responsive structure-Bridged Mesoporous Organosilica Nanomedicine for precise treatment of acute pancreatitis, ACS Nano 18 (29) (2024) 19283–19302, https://doi.org/10.1021/acsnano.4c05369.
[54] Z. Zhang, H. Li, Y. Deng, K. Schuck, S. Raulefs, N. Maeritz, Y. Yu, T. Hechler, A. Pahl, V. Fernández-Sáiz, Y. Wan, G. Wang, T. Engleitner, R. Öllinger, R. Rad, M. Reichert, K.N. Diakopoulos, V. Weber, J. Li, S. Shen, X. Zou, J. Kleeff, A. Mihaljevic, C.W. Michalski, H. Algül, H. Friess, B. Kong, AGR2-Dependent nuclear Import of RNA polymerase II Constitutes a specific target of pancreatic Ductal Adenocarcinoma in the context of Wild-type p53, Gastroenterology 161 (5) (2021) 1601–1614.e23, https://doi.org/10.1053/j.gastro.2021.07.030.
[55] X. Zhou, X. Cao, H. Tu, Z.R. Zhang, L. Deng, Inflammation-targeted delivery of Celastrol via neutrophil membrane-coated nanoparticles in the management of acute pancreatitis, Mol. Pharm. 16 (3) (2019) 1397–1405, https://doi.org/10.1021/acs.molpharmaceut.8b01342.
[56] Y. Huangfu, X. Yu, C. Wan, Y. Zhu, Z. Wei, F. Li, Y. Wang, K. Zhang, S. Li, Y. Dong, Y. Li, H. Niu, G. Xin, W. Huang, Xanthohumol alleviates oxidative stress and impaired autophagy in experimental severe acute pancreatitis through inhibition of AKT/mTOR, Front. Pharmacol. 14 (2023) 1105726, https://doi.org/10.3389/fphar.2023.1105726.
[57] M.W. Liu, R. Wei, M.X. Su, H. Li, T.W. Fang, W. Zhang, Retraction Note: effects of Panax notoginseng saponins on severe acute pancreatitis through the regulation of mTOR/Akt and caspase-3 signaling pathway by upregulating miR-181b expression in rats, BMC Complement Med Ther 22 (1) (2022) 306, https://doi.org/10.1186/s12906-022-03799-4.
[58] Y. Liao, J. Xu, B. Qin, J. Shi, C. Qin, F. Xie, S. Ou, J. Tang, W. Wang, F. Wu, L. Bai, Advanced oxidation protein products impair autophagic flux in macrophage by inducing lysosomal dysfunction via activation of PI3K-Akt-mTOR pathway in Crohn's disease, Free Radic. Biol. Med. 172 (2021) 33–47, https://doi.org/10.1016/j.freeradbiomed.2021.05.018.
[59] X.D. Wang, W.L. Yu, Y. Sun, Activation of AMPK restored impaired autophagy and inhibited inflammation reaction by up-regulating SIRT1 in acute pancreatitis, Life Sci. 277 (2021) 119435, https://doi.org/10.1016/j.lfs.2021.119435.
[60] J. Liu, Y. Yang, X. Liu, A.S. Widjaya, B. Jiang, Y. Jiang, Macrophage-biomimetic anti-inflammatory liposomes for homing and treating of aortic dissection, J. Contr. Release 337 (2021) 224–235, https://doi.org/10.1016/j.jconrel.2021.07.032.